〔Articles〕

Improvement in Automobile Maneuverability and Stability through Chassis Integrity Control System

Kazunori MORI*

Abstract

We propose a method to cooperatively control the right and left torque distribution system of braking/driving forces, the four-wheel-steering and the active suspension cooperatively to concurrently improve maneuverability/stability and ride comfort for automobiles. Using the LQ control theory, we obtained the integrity control rule by which both the body slip angle and the yaw rate characteristics to steering input were made not only to follow the target values, but also control the swing of the body. Computer simulation confirmed that when the vehicle applied this chassis integrated control system, the effects of control for improving the vehicle performance were greater than that of the active suspension control alone. In addition, our data suggest that this system makes it possible to achieve good control effects under bad conditions such as a variety of rugged roads and the μ turbulence roads. Moreover, because this system can greatly decrease the amount of steering work required of the driver, a reduction in physical and mental load can also be expected.

Key Words: Automobile, Vehicle Dynamics, Motion Control, Integrity Control System, Simulation, Braking/Driving System, Four-Wheel-Steering, Active Suspension, Maneuverability, Stability

1. Introduction

Though the improvement of active safety is expected for the automobile, improved riding comfort is also requested. Therefore we should make the contradictory performances of both maneuverability/stability and riding comfort united at the higher level. So far, a lot of chassis control systems such as VDC, four-wheel steering and active suspension have been put to practical use[(1)-(3)]. These systems have improved the maneuverability/stability or the riding comfort by individually controlling the three directional tire forces (longitudinal, lateral and upper/lower forces) or the input forces to suspension apparatus, which are directly influenced in the performance of vehicle dynamics. Recently, new methods have been proposed to concurrently control the two directional tire forces acting on four wheels[(4)-(6)]. In addition, if all three direction forces working on tires are cooperatively controlled by the state of the running scene and the vehicle while integratedly administering the chassis system and the power system, it may become easier to control the driving operation further, with passengers' comfort being improved simultaneously under various road surface conditions.

In this report, we propose an applied method of the optimum control theory to control the tire forces in three directions cooperatively. And computer simulation clarifies that the chassis device, which integrates and controls the right and left torque distribution system of braking/driving forces, the four-wheel-steering and the active suspension through this method, can concurrently improve maneuverability/stability and ride comfort for automobiles under severe running conditions to corner with braking on the undulation road, etc.

* 交通機械工学科
平成19年4月17日受理

2. Nomenclature

The main notations used in this paper are listed below.

C_j: cornering power of tire

C_{Ri}: ratio of steer angle to roll angle

F_{aj}: power where actuator is generated

F_{jx}, F_{jy}, F_{jz}: tire force in x, y, z axis direction at each wheel position

F'_{jz}: force acting on unsprung mass because of tire

G_{r0}: target value of steady yaw rate gain

I_i: moment of inertia around axis of wheel

I_x, I_y, I_z: roll, pitch, yaw moment of inertia

K_{i0}: cornering power at standard tire load W_{i0}

K_{st}: steering stiffness

M: direct yaw moment generated by right/left wheel torque distribution

$M_{\phi i}$: moment of resistance of roll

N: steering overall gear ratio

R: effective radius of tire

S_{ki}: roll stiffness element with stabilizer

T_j: braking/driving torque acting on tire

W_j: tire load

a, b: distance from front/rear axle to center of gravity of vehicle

c_i: damping coefficient in vertical direction of suspension

c_{ti}: damping coefficient in vertical direction of tire

e: distance from yawing center to c.g. (rear side of c.g.)

g: acceleration due to gravity

h_{cg}: vehicle height at c.g.

h_{RC}: height of roll center at c.g.

h_i: height of roll center at front/rear axle

h_s: rolling moment arm length

k_i: spring constant in vertical direction of suspension

k_{ti}: spring constant in vertical direction of tire

l: wheelbase

m, m_s, m_i: vehicle mass, sprung mass, unsprung mass

r, r_m: yaw rate, target yaw rate

s, s_j: Laplace transform operator, tire slip ratio

t, t_c: time, caster trail of front wheel

t_i: front/rear wheel tread

u_j, u_{0j}: vertical displacement of body at each wheel position, road displacement

v, v_j, $v_{j\omega}$: vehicle velocity, body velocity at tire center position of each wheel, velocity component in direction of tire centerline

u'_j: vertical displacement of unsprung at each wheel position

α_x, α_y, α_z: longitudinal, lateral, vertical acceleration at c.g. of vehicle

β: body sideslip angle at at c.g. of vehicle

β_j, β_m: tire sideslip angle, target body sideslip angle
δ_{ci}: compliance steer due to longitudinal and lateral forces
δ_f: front wheel steer angle on maneuvering steering wheel
δ_{Ri}: roll steer
δ_j: wheel steer angle
δ_{ra}: active steer angle of rear wheel
ε_j, ε'_j: wheel stroke, vertical displacement of tire
θ: steering wheel angle $\delta_f=\theta/N$
λ: pitch angle, undecided multiplier of Lagrange
μ_s, μ_d: coefficient of road-tire static friction, coefficient of road-tire dynamic friction
ρ_i: link lever ratio of suspension
ϕ: roll angle
τ_r: time coefficient of first order delay on target yaw rate characteristics
ω_j: rotating angle velocity of tire
o-xyz, O−XYZ: coordinates fixed to the vehicle body, coordinates fixed to the road
Subscripts
i: f-front wheels, r-rear wheels
j: 1-right front wheel, 2-right rear wheel, 3-left front wheel, 4-left rear wheel
0: initial state variable

3. Equations of motion

Figure 1 shows the calculating model for the analysis of vehicle dynamics. This model is shown by 14 degrees of freedom in which the vertical movement of the unsprung mass and the rotary motion of the wheel, in addition to the rotary motion and the translation to three coordinate axis of the body are considered. Moreover, the simplification of the expression is aimed at the assumption of the following contents. All product of inertia around the coordinates fixed to the body is zero. The roll center, containing the middle point of the line where a right and left wheel are connected, is located on vertical plane for the road and fixed to the body.

When the equation of vehicle motion is led with the coordinate system fixed to the body, the translation is shown as follows.

$$m\alpha_x=\sum F_{jx} \tag{1}$$
$$m\alpha_y=\sum F_{jy}+m_s h_s\ddot{\phi} \tag{2}$$
$$m\alpha_z=\sum F_{jz} \tag{3}$$

Then acceleration of each direction is described by

$$\left.\begin{aligned}\alpha_x&=\ddot{x}-\dot{y}r+z\dot{\lambda}\\ \alpha_y&=\ddot{y}+\dot{x}r-z\dot{\phi}\\ \alpha_z&=\ddot{z}-\dot{x}\dot{\lambda}+y\dot{\phi}\end{aligned}\right\} \tag{4}$$

The balance type of the moment around the roll, the pitch, and the yaw axis is shown respectively as follows.

$$I_x\ddot{\phi}-m_s h_s\alpha_y-m_s h_s g\phi=M_{\phi f}+M_{\phi r} \tag{5}$$
$$I_y\ddot{\lambda}+mh_{cg0}\alpha_x=-a(F_{1z}+F_{3z})+b(F_{2z}+F_{4z}) \tag{6}$$
$$I_z\dot{r}=a(F_{1y}+F_{3y})-b(F_{2y}+F_{4y})+M \tag{7}$$

The direct yaw moment is expressed by

$$M=t_f(F_{1y}-F_{3y})/2+t_r(F_{2y}-F_{4y})/2 \tag{8}$$

Various expressions for the roll motion in Eq. (5) are recorded in this paper's appendix.

The front and rear steer angles are described by

$$\left.\begin{aligned}\delta_1&=\delta_f-(t_c+t_{pf})(F_{1y}+F_{3y})/K_{st}+\delta_{Rf}+\delta_{cf}\\ \delta_2&=\delta_{Rr}+\delta_{cr}+\delta_{ra}\\ \delta_3&=\delta_f-(t_c+t_{pf})(F_{1y}+F_{3y})/K_{st}-\delta_{Rf}+\delta_{cf}\\ \delta_4&=-\delta_{Rr}+\delta_{cr}+\delta_{ra}\end{aligned}\right\} \tag{9}$$

where roll steer δ_{Ri} is a function of ε_j, compliance steer δ_{ci} is a function of F_{jx} and F_{jy}. In the same way, camber angle γ_j is shown as a function of δ_{ci}, F_{jx} and F_{jy}.

Tire slip angles of each wheel are given as follows.

$$\left.\begin{aligned}\beta_1&=\delta_1-\tan^{-1}((\dot{y}+ar)/v\\ \beta_2&=\delta_2-\tan^{-1}((\dot{y}-br)/v\\ \beta_3&=\delta_3-\tan^{-1}((\dot{y}+ar)/v\\ \beta_4&=\delta_4-\tan^{-1}((\dot{y}-br)/v\end{aligned}\right\} \tag{10}$$

The rotary motions of each wheel are shown by the next equations.

$$I_i\dot{\omega}_j=T_j-F_{jx}R \quad (1\leq j\leq 4) \tag{11}$$

The expression for the slip ratio of tire is recorded in the appendix.

The displacement of the sprung mass and the displacement of the unsprung mass are shown respectively by Eq. (12) and Eq. (13).

$$\left.\begin{aligned}u_1&=z-a\lambda-t_f\phi/2\\ u_2&=z+b\lambda-t_r\phi/2\\ u_3&=z-a\lambda+t_f\phi/2\\ u_4&=z+b\lambda+t_r\phi/2\end{aligned}\right\} \tag{12}$$

$$\left.\begin{aligned}\varepsilon_j&=u_j-u'_j\\ \varepsilon'_j&=u'_j-u_{0j}\end{aligned}\right\} \tag{13}$$

The balance type of force for the sprung mass is shown respectively as follows.

$$\left.\begin{aligned}F_{1z}&=-k_f\varepsilon_1-c_f\dot{\varepsilon}_1-F_{a1}-S_{kf}(\varepsilon_1-\varepsilon_3)/t_f^2\\ F_{2z}&=-k_r\varepsilon_2-c_r\dot{\varepsilon}_2-F_{a2}-S_{kr}(\varepsilon_2-\varepsilon_4)/t_r^2\\ F_{3z}&=-k_f\varepsilon_3-c_f\dot{\varepsilon}_3-F_{a3}-S_{kf}(\varepsilon_3-\varepsilon_1)/t_f^2\\ F_{4z}&=-k_r\varepsilon_4-c_r\dot{\varepsilon}_4-F_{a4}-S_{kr}(\varepsilon_4-\varepsilon_2)/t_r^2\end{aligned}\right\} \tag{14}$$

The balance type of force for the unsprung mass of each wheel is shown as follows.

$$\left.\begin{aligned}m_f\ddot{u}'_1&=-F_{1z}+F'_{1z}\\ m_r\ddot{u}'_2&=-F_{2z}+F'_{2z}\\ m_f\ddot{u}'_3&=-F_{3z}+F'_{3z}\\ m_r\ddot{u}'_4&=-F_{4z}+F'_{4z}\end{aligned}\right\} \tag{15}$$

Here, force acting on the tire is expressed by.

$$F'_{jz}=-k_{ti}\varepsilon'_j-c_{ti}\dot{\varepsilon}'_j \tag{16}$$

Moreover, vertical direction load of each tire is shown as follows.

$$\left.\begin{aligned}W_1&=bmg/(2l)+F'_{1z}\\ W_2&=amg/(2l)+F'_{2z}\\ W_3&=bmg/(2l)+F'_{3z}\\ W_4&=amg/(2l)+F'_{4z}\end{aligned}\right\} \tag{17}$$

The Sakai's equation considering the slip ratio is used for the expression which shows the relationship between the longitudinal tire

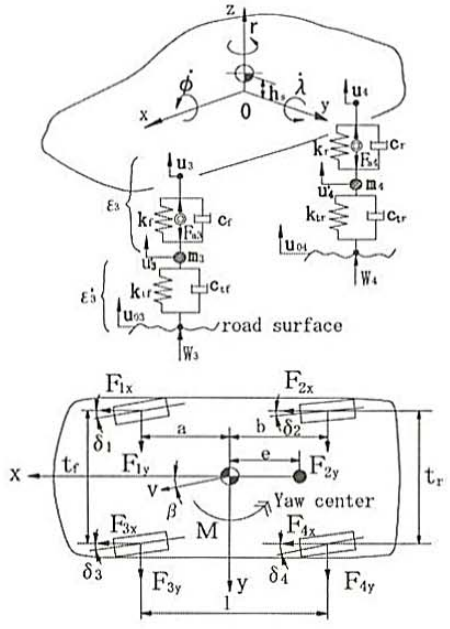

Fig. 1 Vehicle model

force and the lateral tire force. However, because the tire force in executing the calculation should be an odd function for the sideslip angle, a part of Sakai's equation has been changed.

The steering system uses the model of the one degree of freedom system considering the assist force of power steering system[7].

4. Control law

The purpose of the control is provided to bring yaw rate r close to target yaw rate r_m, to adjust the position (yaw center) in which a dynamic sideslip angle of the body becomes zero to a prescribed position, and to bring roll angle ϕ, pitch angle λ, and bouncing z close to zero to reduce the swing of the body and the vertical motion.

When the controller is designed, rotary motion of the vehicle model in the preceding chapter is simplified as much as possible to facilitate the calculation of the control system. Then, it is assumed that the movement of unsprung mass and the rotary motion of road wheel are not considered. In addition, the influence of tire slip ratio and compliance steer element in suspension characteristics are disregarded. The simplified equations of motion are expressed in the form of a state equation, and the following equation is obtained.

$$\dot{\mathbf{x}}=\mathbf{A}\mathbf{x}+\mathbf{B}\mathbf{u}+\mathbf{E}\delta_f+\mathbf{w} \tag{18}$$

where

$$\mathbf{x}=[\beta\ r\ \dot{\phi}\ \phi\ \dot{\lambda}\ \lambda\ \dot{z}\ z]^T$$
$$\mathbf{u}=[\delta_r\ M\ F_{a1}\ F_{a2}\ F_{a3}\ F_{a4}]^T$$
$$\mathbf{w}=[0\ 0\ 0\ 0\ -mh_{cg0}\alpha_x/I_y\ 0\ 0\ 0]^T$$

A, B, and E are decided by the vehicle, the tire characteristics, and the velocity of vehicle, and are the matrix dimensions of (8×6), (8×6), and (8×1) respectively. Both x and w are enabled to be detected.

To operate the control law easily, it is assumed that the influences of elements a_{31} and a_{32} of A are less than other elements and put and calculated with zero. In addition, it is assumed that the steer angle element influences neither element b_{31} of B nor e_{31} of E and puts it with zero. Therefore, it is possible to describe it by progressing Eq. (18) as in the next equations.

$$\dot{\mathbf{x}}_1=\mathbf{A}_{11}\mathbf{x}_1+\mathbf{A}_{12}\mathbf{x}_2+\mathbf{B}_{11}\mathbf{u}_1+\mathbf{E}_1\delta_f \tag{19}$$
$$\dot{\mathbf{x}}_2=\mathbf{A}_{22}\mathbf{x}_2+\mathbf{B}_{22}\mathbf{u}_2+\mathbf{w}_2 \tag{20}$$

where

$$\mathbf{x}_1=[\beta\ r]^T,\ \mathbf{x}_1=[\dot{\phi}\ \phi\ \dot{\lambda}\ \lambda\ \dot{z}\ z]^T,\ \mathbf{u}_1=[\delta_r\ M]^T,\ \mathbf{u}_2=[F_{a1}\ F_{a2}\ F_{a3}\ F_{a4}]^T$$

and

$$\mathbf{A}=\begin{bmatrix}\mathbf{A}_{11} & \mathbf{A}_{12}\\ 0 & \mathbf{A}_{22}\end{bmatrix}\quad \mathbf{B}=\begin{bmatrix}\mathbf{B}_{11} & 0\\ 0 & \mathbf{B}_{22}\end{bmatrix}$$
$$\mathbf{E}=\begin{bmatrix}\mathbf{E}_1\\ 0\end{bmatrix}\quad \mathbf{w}=\begin{bmatrix}0\\ \mathbf{w}_2\end{bmatrix}$$

When the distance between yaw center position and center of gravity is defined as e, $\beta=er/v$.

Using this equation, the target characteristics of body sideslip angle and yaw rate are given by the following transfer functions[8].

$$\beta_m=er_m/v \tag{21}$$
$$\frac{r_m}{\delta_f}=\frac{G_{r0}}{1+\tau_r s} \tag{22}$$

Here, Eqs. (21)-(22) are represented in the form of a state equation as follows.

$$\dot{\mathbf{x}}_{1m}=\mathbf{A}_{11m}\mathbf{x}_{1m}+\mathbf{E}_{1m}\delta_f \tag{23}$$

where

$$\mathbf{x}_{1m}=[\beta_m \quad r_m]^T$$

Then $\mathbf{e}=\mathbf{x}_1-\mathbf{x}_{1m}$, the error margin equation is derived by using Eq. (19) and Eq. (23).

$$\dot{\mathbf{e}}=\mathbf{A}_{11}\mathbf{e}+\mathbf{B}_{11}\mathbf{u}_{1b}+\mathbf{A}_{12}\mathbf{x}_2 \tag{24}$$

Here, $\mathbf{u}_{1b}$ is the feedback term of $\mathbf{u}_1$. The second term of right side is given by Eq. (25).

$$\mathbf{B}_{11}\mathbf{u}_{1b}=(\mathbf{A}_{11}-\mathbf{A}_{11m})\mathbf{x}_{1m}+\mathbf{B}_{11}\mathbf{u}_1+(\mathbf{E}_1-\mathbf{E}_{1m})\delta_f \tag{25}$$

It is shown that Eq. (20) and Eq. (24) are brought together by the next equation.

$$\dot{\tilde{\mathbf{x}}}=\mathbf{A}\tilde{\mathbf{x}}+\mathbf{B}\tilde{\mathbf{u}}+\mathbf{w} \tag{26}$$

where

$$\tilde{\mathbf{x}}=\begin{bmatrix}\mathbf{e}\\ \mathbf{x}_2\end{bmatrix} \qquad \tilde{\mathbf{u}}=\begin{bmatrix}\mathbf{u}_{1b}\\ \mathbf{u}_2\end{bmatrix}$$

Eq. (26) is handled as the optimum regulator problem, and $\tilde{\mathbf{u}}$ that can minimize the performance function J is derived[9].

$$J=\int_0^\infty(\tilde{\mathbf{x}}^T\mathbf{Q}\tilde{\mathbf{x}}+\tilde{\mathbf{u}}^T\mathbf{R}\tilde{\mathbf{u}})dt \tag{27}$$

Here, Q and R are the arbitrary weight putting constant matrix.

The procedure for requesting $\tilde{\mathbf{u}}$ is shown.

Hamiltonian H is expressed by the next equation now.

$$H=L+\lambda^T\mathbf{f} \tag{28}$$

where

$$\left.\begin{aligned}L&=\tilde{\mathbf{x}}^T\mathbf{Q}\tilde{\mathbf{x}}+\tilde{\mathbf{u}}^T\mathbf{R}\tilde{\mathbf{u}}\\ \mathbf{f}&=\mathbf{A}\tilde{\mathbf{x}}+\mathbf{B}\tilde{\mathbf{u}}+\mathbf{w}\end{aligned}\right\}$$

λ shows the undecided multiplier vector of Lagrange.

By the Euler equation, the necessary condition that made J minimum is shown by the next equations.

$$\left.\begin{aligned}\dot{\lambda}&=-\left(\frac{\partial H}{\partial\tilde{\mathbf{x}}}\right)^T=-(\mathbf{Q}\tilde{\mathbf{x}}+\mathbf{A}^T\lambda)\\ \frac{\partial H}{\partial\tilde{\mathbf{u}}}&=\mathbf{R}\tilde{\mathbf{u}}+\mathbf{B}^T\lambda=0\\ \dot{\tilde{\mathbf{x}}}&=\left(\frac{\partial H}{\partial\lambda}\right)^T=\mathbf{A}\tilde{\mathbf{x}}+\mathbf{B}\tilde{\mathbf{u}}+\mathbf{w}\end{aligned}\right\} \tag{29}$$

It is assumed that λ becomes the shape of Eq. (30).

$$\lambda=\mathbf{P}\tilde{\mathbf{x}}+\mathbf{P}_1\mathbf{w} \tag{30}$$

By the second equation of Eq. (29), $\tilde{\mathbf{u}}=-\mathbf{R}^{-1}\mathbf{B}^T\lambda$ is obtained. Substituting Eq. (30) into this equation, next Eq. (31) is obtained.

$$\tilde{\mathbf{u}}=-\mathbf{R}^{-1}\mathbf{B}^T(\mathbf{P}\tilde{\mathbf{x}}+\mathbf{P}_1\mathbf{w}) \tag{31}$$

Assuming that w is constant vector, the following relations are derived by some equations led from Eq. (29) and the equation that differentiated both sides of Eq. (30) at time.

$$\dot{\mathbf{P}}+\mathbf{PA}-\mathbf{PBR}^{-1}\mathbf{B}^T\mathbf{P}+\mathbf{Q}+\mathbf{A}^T\mathbf{P}=0 \tag{32}$$

$$\mathbf{P}_1=(\mathbf{PBR}^{-1}\mathbf{B}^T-\mathbf{A}^T)^{-1}\mathbf{P} \tag{33}$$

Eq. (32) is Riccati equation to P known well. P is obtained by solving Eq. (32). This is substituted for Eq. (33) and $\mathbf{P}_1$ is obtained.

Therefore, $\tilde{\mathbf{u}}$ is decided by equation (31).

Next, it is defined that sum with feed forward term $\mathbf{u}_{1f}$ and feedback term $\mathbf{u}_{1b}$ (the element of $\tilde{\mathbf{u}}$) is $\mathbf{u}_1$.

$$\mathbf{u}_1=\mathbf{u}_{1f}+\mathbf{u}_{1b} \tag{34}$$

Substituting Eq. (34) into Eq. (25), $\mathbf{u}_{1f}$ is derived as follows.

$$\mathbf{u}_{1f}=-\mathbf{B}_{11}^{-1}\{(\mathbf{A}_{11}-\mathbf{A}_{11m})\mathbf{x}_{1m}+(\mathbf{E}_1-\mathbf{E}_{1m})\delta_f\} \tag{35}$$

Therefore, using Eqs. (31), (34), and (35), the control law is shown by the next equation.

$$\mathbf{u}=\left[\begin{array}{c}-\mathbf{B}_{11}^{-1}\left\{(\mathbf{A}_{11}-\mathbf{A}_{11m})\begin{bmatrix}\beta_m\\ r_m\end{bmatrix}+(\mathbf{E}_1-\mathbf{E}_{1m})\delta_f\right\}\\ \mathbf{0}\end{array}\right]-\mathbf{R}^{-1}\mathbf{B}^T\left\{\mathbf{P}\begin{bmatrix}\mathbf{e}\\ \mathbf{x}_2\end{bmatrix}+(\mathbf{PBR}^{-1}\mathbf{B}^T-\mathbf{A}^T)^{-1}\mathbf{Pw}\right\} \tag{36}$$

The first term in the right side of Eq. (36) shows the steering angle feedforward term and the second term shows the state feedback term.

5. Calculation and consideration

Maneuverability and stability of a vehicle through the integrated control of three direction forces on the tires (called XYZ control in this paper) are compared with those of the active suspension (called Z control) and conventional vehicle (called vehicle without control) by computer simulation. The control law of XYZ control uses the proposed control functions that are determined so that the yaw center can coincide with the vehicle's center of gravity at all times, and the objective steady yaw rate gain G_{r0} can be equal to that of vehicle without control at $\alpha_x=0$ in Eqs. (21) and (22). We set up that the time constant of first-order delay τ_r is 0.035 second. Moreover, when the direct yaw moment M is distributed as the longitudinal force of wheels, the distribution ratio of longitudinal force adopts the method of proportion to tire weight distribution ratio[10]. We set $\mathbf{Q}=\mathrm{diag}(250, 30, 1, 1, 1, 1, 1, 1)$ and $\mathbf{R}=\mathrm{diag}(300, 1.1\times10^{-8}, 1.0\times10^{-8}, 1.0\times10^{-8}, 1.0\times10^{-8}, 1.0\times10^{-8})$ in Eq. (27). These weighting matrices are constant to the change in the vehicle velocity and the state of road surface. The specifications of a typical compact passenger vehicle of 4WD are used in simulations. We carried out computational simulation using the direct numerical integration of the vehicle and the steering wheel model in Chapter 3.

5.1 Control response from steady circular turning

Figure 2 shows the response characteristics for the step steer of increase steering angle 15 deg that is executed from the state of steady circular turning with steering angle 30 deg and braking deceleration 0.3 G at initial vehicle velocity 120 km/h. We perform the calculation under the quasi-steady state assuming that the elapsed time is extremely short in order to neglect the fluctuation of vehicle velocity due to longitudinal acceleration and deceleration. As for XYZ control, the standing up of the yaw rate and lateral acceleration to steering input is earlier than that of Z control and without control. Moreover, the transient overshoot is also less. The performance gain of the steering effort is also moderately large, and a so-called "steering works well" is obtained. Yaw rate follows well for the target characteristic, though the initial steady value becomes small by the influence with deceleration. And, the characteristic of body sideslip angle doesn't generate the transient overshoot and is also steady. As for the swing of the body, it almost becomes zero the same as the target value, and both XYZ control and Z control obtain an extremely excellent result.

5.2 Influence of turbulence by ruggedness of road

① Cornering on undulation road

We investigate the maneuverability and stability of the case that the driver steers and brakes by going into the undulation road from the state for turning around a smooth road at the steering angle 30 deg and vehicle velocity 100 km/h. The driver adds the step steer two seconds after the calculation beginning and the deceleration of 0.3 G will be added in three seconds. The ruggedness amplitude is set to be 0.015 m on the undulation road. To become bad condition for upper and lower swing, the road ruggedness cycle is determined to be 22.3 m matching the natural frequency on the sprung mass to the time frequency of the road. The displacement input between right and left

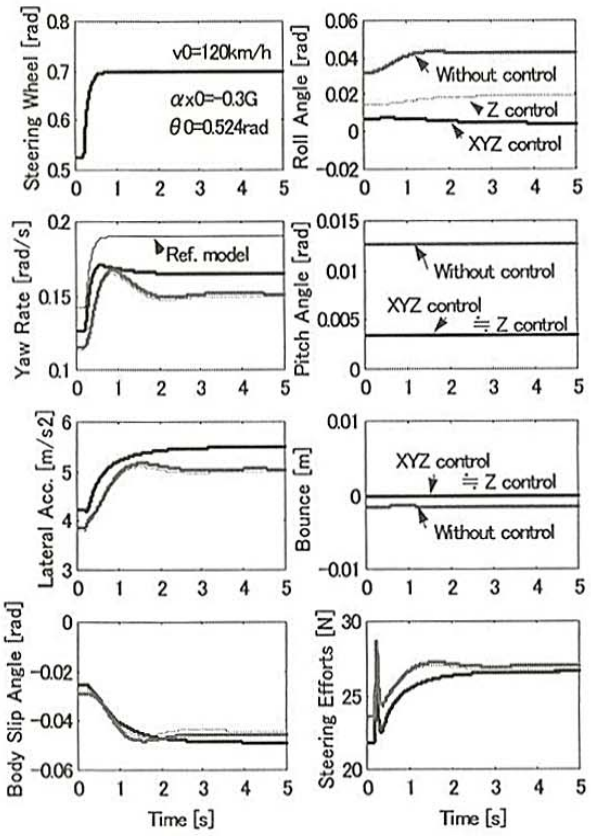

Fig. 2 Step response characteristics

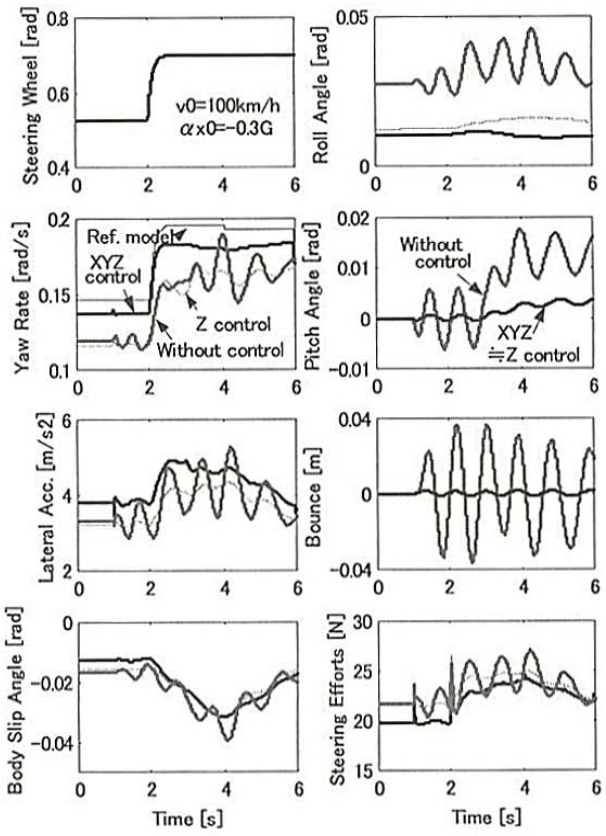

Fig. 3 Vehicle motion on the undulated road

wheels to the road is set to be the same phase. Figure 3 shows the calculation result. The effect of XYZ control and Z control is large when there is road ruggedness turbulence of the traveling direction. Especially, the effect of the XYZ control grows more than Z control when running on the undulation road of the curve like the calculation.

② Lane change to rut road

Next, in order to investigate the influence of turbulence by the crossing direction ruggedness of the road, we carry out the simulation in which the driver is asked to execute going into the rut road by changing the lane during the deceleration 0.3 G at the initial vehicle velocity 120 km/h. We apply the first-order prediction model using the feedback of lateral error from a desired course to the driver's model. Figure 4 shows the running route and the road cross-sectional view of the rut road. We set the depth d of rut moat is 0.04 m, the width W of rut moat is 0.9m, and the distance D of both rut moat center is 1.49 m in the calculation. Figure 5 and Figure 6 show the calculation result. XYZ control can suppress the influence of the lateral force turbulence by the change of camber angle to the ground and of tire load caused by the ragged road, and achieve to change the lane steady also on the rut road as well as the case of a smooth road. The control effect of XYZ control is larger than that of Z control.

We consider that the driver's operating workload decreases due to stabilization of the driver's field of vision, so that the swing of the body may decrease on the undulation road and the rut road when the XYZ control is applied to the vehicle.

As for the amount of the input, of the active control in the vertical direction, neither XYZ control nor Z control are very different.

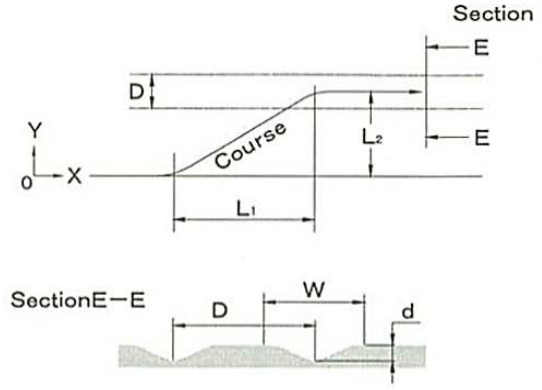

Fig. 4 Rut surface road

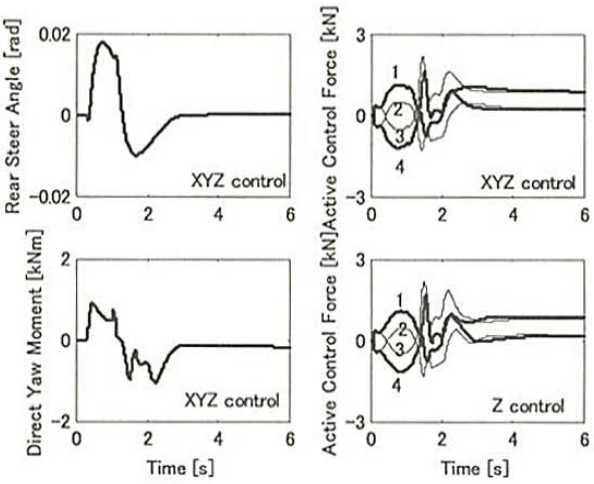

Fig. 6 Control input on the rut road

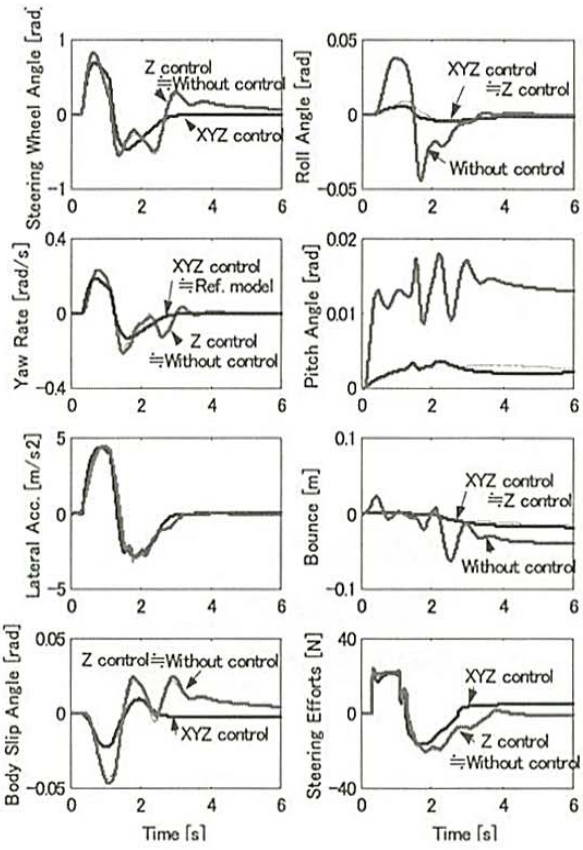

Fig. 5 Vehicle motion on the rut road

5.3 Influence of change in friction coefficient of road

The split μ street-running used for the evaluation of the braking stability is simulated. The coefficient of dynamic friction of the high μ road and the low μ road is set to be 0.8 and 0.14 respectively. After it goes straight in initial velocity by 30 m as 120 km/h, it brakes by deceleration 0.3 G. Afterwards, to go into the split μ road so that the left wheels may become on the low μ road, and the driver steers the steering wheel to keep going straight. The driver model is the same as the foregoing paragraph. Figure 7 and Figure 8 show the calculation result. The vehicle through XYZ control also causes neither staggering nor a lateral movement, and it is possible to go straight in XYZ control by a little amount of the correction steer. There is little control effect to directional stability though Z control, and the swing of the body is small.

5.4 Necessary work for steering wheel maneuver

To examine the driver's physical load, the workload that the driver did to the steering wheel is calculated. Here, it is defined with the workload as the value in which the product of the angular velocity of the steering wheel and the steering effort is integrated in a certain fixed time section. Figure 9 shows the workload of the driver of each control specification when running on the rut road and the split μ road in the foregoing paragraph. Six seconds from the calculation beginning to the end are set as a section of the time to request the workload. Moreover, the result of the split μ running multiplies 30 and showed the workload in the figure. It is confirmed that the driver's load of XYZ control is the smallest as well as the result of the foregoing paragraph.

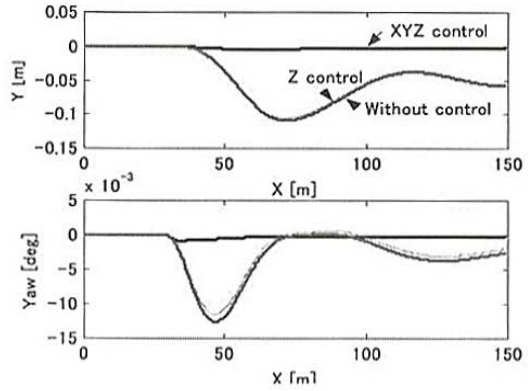

Fig. 7 Lateral displacement and yaw angle

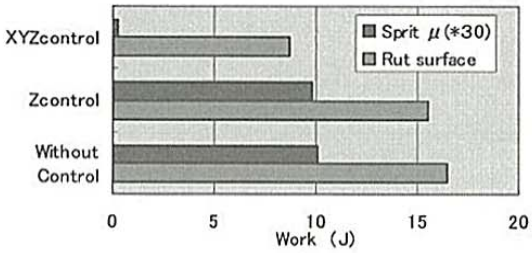

Fig. 9 Comparison of Driver's workload

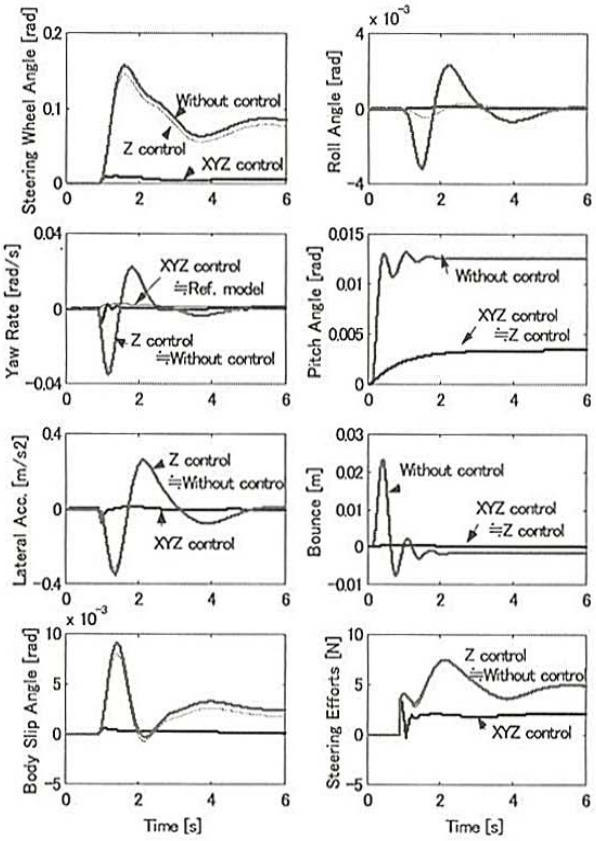

Fig. 8 Vehicle motion on the sprit μ road

6. Conclusions

We examined a method to cooperatively control the three directional forces upon the vehicle by the chassis device which integrates and controls the right and left torque distribution system of braking/driving forces, the four -wheel-steering and the active suspension. Computer simulation clarified this control effect, and the following results are obtained.

(1) We obtained the control law integrated chassis systems by applying LQ control theory. This control law makes the yaw rate characteristic to the steering wheel angle follow to target, and adjusts the yaw center to an expected position, and further enables the suppression of the body swing.

(2) As for the vehicle applied with the control systems of (1), the effect to the performance improving is large only in case of the active suspension control.

・The steer response stability and riding comfort can be united in the higher dimension by using this control in the running scene under a bad condition such as a variety of ruggedness roads and the μ turbulence roads.

・Because the workload to the driver's steering maneuver can be greatly decreased, the reduction of not only a physical load but also a mental load is expected.

・The amount of the control input changes by the running scene, and it has been understood not to become a decrease of all energy consumptions in the control systems of the proposal.

This research aimed to examine a technical possibility theoretically. Therefore, we executed the simulation calculation, assumed that there was no delay characteristics on the system and all state variables were able to be detected. The following problems include the confirmation of the control effect when the delay of the device and

the nonlinear factor are considered, the design consideration of the control system that applies the observer, and so on.

Appendix

1. Explanation of equations:

■ In Eq. (5)

$$M_{\phi f}=-t_f(F_{1z}-F_{3z})\rho_f/2,\quad M_{\phi r}=-t_r(F_{2z}-F_{4z})\rho_r/2$$

$$h_{RC}=(bh_f+ah_r)/l$$

$$h_{cg}=h_{RC}+h_s=h_{cg0}+z,\quad h_f=h_{f0}+z,\quad h_r=h_{r0}+z$$

■ The slip ratio of the tire in Eq. (11) is defined as follows.

At braking: $s_j=(v_{j\omega}-R\omega_j)/v_{j\omega}$ At drive: $s_j=-(R\omega_j-v_{j\omega})/R\omega_j$

Here, it is assumed $v_{j\omega}\approx v_j$.

where

$$\left.\begin{aligned} v_1&=\dot{x}+t_f r/2,\quad v_2=\dot{x}+t_r r/2\\ v_3&=\dot{x}-t_f r/2,\quad v_4=\dot{x}-t_r r/2 \end{aligned}\right\}$$

■ Cornering characteristics of tire (for analytical calculation of vehicle dynamics):

$$\begin{aligned} F_{jx}&=-\mathrm{sgn}(s_j)\mu_{dj}W_j && :|s_j|=1\\ &=-\{(K_j(1-q_j)^2+\mu_{dj}W_jq_j^2(3-2q_j)h_j\}s_j && :|s_j|<1\\ F_{jy}&=K_j(1-s_j)^2(1-q_j^2)\tan\beta_j+\mu_{dj}W_jq_j^2(3-2q_j)h_j\tan\beta_j && :-1\le s_j\le 0\\ &=K_j(1-s_j)(1-q_j^2)\sin\beta_j+\mu_{dj}W_jq_j^2(3-2q_j)h_j\tan\beta_j && :0<s_j\le 1 \end{aligned}$$

Cornering power is defined to be a function of the tire load.

$$K_j=\mu_{dj}K_{i0}\left\{\frac{4}{3}\left(\frac{W_j}{W_{i0}}\right)-\frac{1}{3}\left(\frac{W_j}{W_{i0}}\right)^2\right\}$$

K_{i0} is a value in which the cornering power when the tire load is reference value W_{i0} is divided by μ_d.

In the above-mentioned equations to the cornering characteristics of tire

$$h_j=1/\sqrt{s_j^2+\tan^2\beta_j}$$

$$q_j=K_j\sqrt{s_j^2+\tan^2\beta_j}/(3\mu_{sj}W_j)$$

■ In Eq. (18)

The elements a_{ij}, b_{ij}, e_{ij} of matrix **A**, **B** and **E** are as follows.

$$a_{11}=-(C_{pf}+C_{pr})/mv,\quad a_{12}=(bC_{pr}-aC_{pf})/mv^2-1$$

$$a_{14}=-(C_{pf}C_{Rf}t_f+C_{pr}C_{Rr}t_r)/2mv$$

$$a_{16}=\{-a(C_1-C_3)C_{Rf}+b(C_2-C_4)C_{Rr}\}/mv$$

$$a_{18}=\{(C_1-C_3)C_{Rf}+(C_2-C_4)C_{Rr}\}/mv$$

$$a_{21}=(bC_{pr}-aC_{pf})/I_z,\quad a_{22}=-(a^2C_{pf}+b^2C_{pr})/I_zv$$

$$a_{24}=(-aC_{pf}C_{Rf}t_f+bC_{pr}C_{Rr}t_r)/2I_z$$

$$a_{26}=-\{a^2(C_1-C_3)C_{Rf}+b^2(C_2-C_4)C_{Rr}\}/I_z$$

$$a_{28}=\{a(C_1-C_3)C_{Rf}+b(C_2-C_4)C_{Rr}\}/I_z$$

$$a_{31}=-m_sh_s(C_{pf}+C_{pr})/mI_2$$

$$a_{32}=m_sh_s(bC_{pr}-aC_{pf})/mI_xv$$

$$a_{33}=-(c_ft_f^2+c_rt_r^2)/2I_x$$

$$a_{34}=(2m_sh_sg-k'_ft_f^2-k'_rt_r^2)/2I_x-m_sh_s(C_{pf}C_{Rf}t_f+C_{pr}C_{Rr}t_r)/2mI_x$$

$$a_{36}=m_sh_s\{-a(C_1-C_3)C_{Rf}+b(C_2-C_4)C_{Rr}\}/mI_x$$

$$a_{38}=m_sh_s\{(C_1-C_3)C_{Rf}+(C_2-C_4)C_{Rr}\}/mI_x$$

$$a_{43}=1,\quad a_{55}=-2(a^2c_f+b^2c_r)/I_y$$

$$a_{56}=-2(a^2k_f+b^2k_r)/I_y,\quad a_{57}=2(ac_f-bc_r)/I_y$$

$$a_{58}=2(ak_f-bk_f)/I_y,\quad a_{65}=1$$

$$a_{75}=2(ac_f-bc_r)m_s-v,\quad a_{76}=2(ak_f-bk_r)/m_s$$

$$a_{77}=-2(c_f+c_r)/m_s,\quad a_{78}=-2(k_f+k_r)/m_s,\quad a_{87}=1$$

$$b_{11}=C_{pf}/mv,\quad b_{21}=-bC_{pr}/I_z,\quad b_{31}=m_sh_sC_{pr}/mI_x$$

$$b_{33}=-b_{35}=-t_f/2I_x,\quad b_{34}=-b_{36}=-t_r/2I_x$$

$$b_{53}=b_{55}=-a/I_y,\quad b_{54}=b_{56}=b/I_y$$

$$b_{73}=b_{74}=b_{75}=b_{76}=1/m_s$$

$e_{11}=C_{pf}/mv$, $e_{21}=aC_{pf}/I_z$, $e_{31}=m_s h_s C_{pf}/mI_x$

Other matrix elements are zero.

where

$C_{pf}=C_1+C_3$, $C_{pr}=C_2+C_4$

$k'_f=k_f+2S_f$, $k'_r=k_r+2S_r$

■ In Eqs. (22), (23)

$$G_{r0}=\frac{v}{l(1+K_s v^2)} \qquad K_s=\frac{m}{l^2}\left(\frac{b}{C_{pf}}-\frac{a}{C_{pr}}\right) \quad : \text{Stability factor}$$

$$\mathbf{A}_{11m}=\begin{bmatrix} -\frac{1}{\tau_r} & 0 \\ 0 & -\frac{1}{\tau_r} \end{bmatrix} \qquad \mathbf{E}_{1m}=\begin{bmatrix} \frac{eG_{r0}}{v\tau_r} \\ \frac{G_{r0}}{\tau_r} \end{bmatrix}$$

■ Cornering characteristic of tire (for calculation of controller):

$C_j=K_{j0}\sqrt{1-(a_x/\mu_d g)^2}$

Here, the following relational expressions are used for calculation.

$W_1=bmg/2l-mh_{s0}a_x/2l$

$W_2=amg/2l+mh_{s0}a_x/2l$ $\qquad h_{s0}=h_{cg0}-(h_{f0}b+h_{r0}a)/l$

$W_3=W_1$, $W_4=W_2$

The load shift in right and left wheels is not considered.

2. The main vehicle specifications and tire characteristics used to calculate:

m=1470 (kg), m_s=1270 (kg), $m_1=m_3$=50 (kg), $m_2=m_4$=50 (kg), I_x=550 (kgm²), I_y=1500 (kgm²), I_z=2400 (kgm²), $I_1=I_3$=10 (kgm²), $I_2=I_4$=20 (kgm²), a=1.18 (m), b=1.44 (m), l=2.62 (m), t_f=1.45 (m), t_r=1.46 (m), t_c=0.03 (m), h_{f0}=0.043 (m), h_{r0}=0.095 (m), h_{cg0}=0.49 (m), $C_{Rf}=-0.002$ (rad/rad), C_{Rr}=0.048 (rad/rad), $C_{Sf}=1.57\times10^{-5}$ (rad/N), $C_{Sr}=6.98\times10^{-5}$ (rad/N), (C_{Sf} and C_{Sr} show the compliance steer coefficient.) k_f=20 (kN/m), k_r=20 (kN/m), c_f=3.48 (kNs/m), c_r=2.16 (kNs/m), N=15.4, K_{st}=10.6 (Nm/rad) K_{f0}=40.4 (kN/rad), K_{r0}=60.6 (kN/rad), W_{f0}=3.95 (kN), W_{r0}=3.24 (kN), k_{ti}=180 (kN/m), c_{ti}=10 (kNs/m), R=0.3 (m)

References

(1) Mori, K., Kuroki, J. and Irie, N., Hicas: Advanced 4-Wheel-Steering Systems, S.I.A. paper, No.89040, (1989-10), pp.18-26.

(2) Inoue, H., Naito, G., Matsumoto, S. and Adachi, K., Improvement of Vehicle Dynamics Through State Feedback Control, Pre-print of JSAE, (in Japanese), Vol.944, No.9436305, (1994-10), pp.121-124.

(3) Fukusima, N., Akatsu, Y., Fuzimura, I., Sato, M. and Fukuyama, K., Improvement of high-speed stability and road-hugging by active suspension, Journal of JSAE, (in Japanese), Vol44, No.3, (1990), pp.29-35.

(4) Nagai, M., Yamanaka, S., Saito, Y. and Hirano, Y., Study on Integrated Control of Active Rear Wheel Steering and Braking/Traction Forces, Pre-print of JSAE, (in Japanese),Vol.972, No.9732216, (1997-5), pp.29-32.

(5) Hanamura, Y., Araki, Y., Oya, M. and Harada, H., Control of Maneuverability and Stability as well as Ride Comfort by Active Suspension Control with Additional Vertical Load, Proc. of AVEC '98, 9836310 (1998), pp.117-122.

(6) Harada, M. and Harada, H., Analysis of Lateral Stability with Integrated Control of Suspension and Steering Systems, Trans. Jpn. Soc. Mech. Eng., (in Japanese), Vol.65, No.638, C (1999-10), pp.253-258.

(7) Mori, K., Improvement of Vehicle Dynamics through Integrated Control System of Braking Force Distribution and Four-Wheel-Steering Using Sliding Mode Control Method, Trans. Jpn. Soc. Mech. Eng., (in Japanese), Vol. 68, No.671, C (2002-7), pp.68-74.

(8) Mori, K., Vehicle Cornering Characteristics in Acceleration and Braking through Attitude Control of Front and Rear Tires, JSME Int. Journal, Series C, 39-1 (1996), pp.58-65.

(9) Kato, K., Technological optimum control (approach to nonlinear),University of Tokyo publication association, (in Japanese), (1988), pp.77-102.

(10) Mori, K., Maneuverability and Stability of Vehicles through Control Combined Right/Left Torque Distribution and Four-Wheel-Steering, Trans. Jpn. Soc. Mech. Eng., (in Japanese), Vol.64, No.618, C (1998-2), pp.530-537.